

**Supplementary information for:
Illuminating the spatio-temporal evolution of the
2008-2009 Qaidam earthquake sequence with the joint
use of InSAR time series and teleseismic data.**

Simon Daout¹, Andreas Steinberg^{2,3}, Marius Paul Isken^{2,4}, Sebastian
Heimann⁴, Henriette Sudhaus²

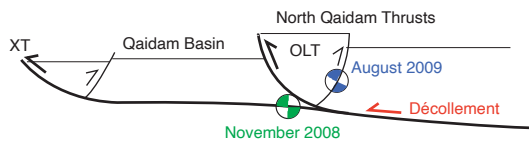
¹COMET, Department of Earth Sciences, University of Oxford, UK

²Christian Albrechts University Kiel, Otto-Hahn-Platz 1, Germany

³Federal Institute for Geosciences and Natural Resources (BGR), Stilleweg 2, 30655 Hannover,
Germany

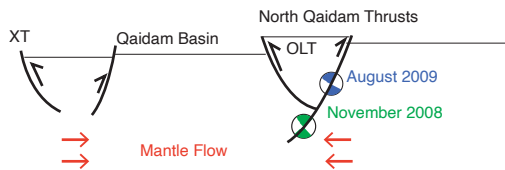
⁴Helmholtz Centre Potsdam, GFZ German Research Centre for Geosciences, Germany

Model 1



- North-dipping thrusts (main planes)/ South-dipping back thrusts
- Transfer of the deformation from north to south through décollements/localised strain-softening zones
- Localised uplift through vertical partitioning

Model 2



- No preferential dipping planes
- Homogeneous uplift driven by mantle/crustal flow
- Homogeneous timing of the deformation from north to south

Figure S1: Simplified sketches summarising the two opposite geodynamic deformation models of northeastern Tibet with their implications for the faults geometry of the North Qaidam thrust system. Numerous other interpretations might fit within those two end-member models. OLT: Olongbulak thrusts. XT: Xietieshan thrusts.

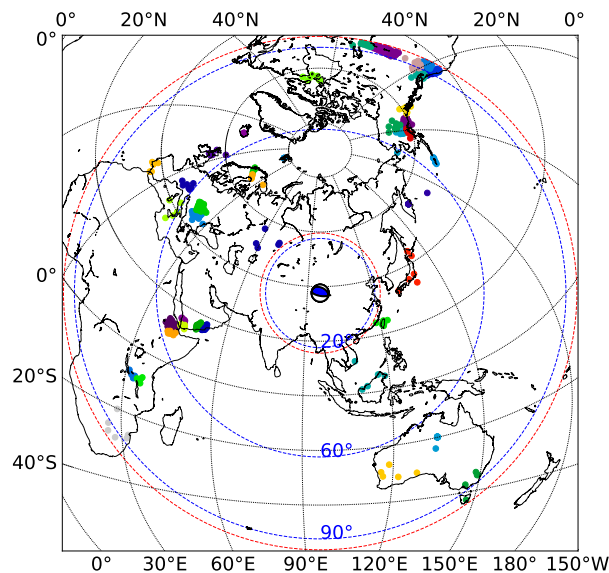


Figure S2: Station array locations used for the backprojection of the 2008 and 2009 earthquakes. Blue lines are distances in degree and red lines are the inner and outer circles of the station selection at 22° and 94°. Stations are colored after the virtual array they belong to.

Table S1: Summary of the gCMT solutions [Ekström *et al.*, 2012] for the 8 $M_w > 5.2$ earthquakes that occurred in Qaidam between 2003 and 2009.

Parameters	2003/04/17	2004/05/04	2004/05/04b	2004/05/10	2008/11/10	2009/08/28	2009/08/30	2009/08/31
Magnitude	6.3	5.3	5.2	5.5	6.3	6.3	5.4	5.8
Depth (km)	16	18.6	21.6	12	27.2	12	16.8	12
Half duration (s)	3.6	1.2	1.0	1.4	3.6	3.3	1.2	3.6
strike1 (°)	294	145	140	272	252	295	272	277
dip1 (°)	29	83	87	33	28	31	45	33
rake1 (°)	88	175	-178	69	57	102	118	90
strike2 (°)	116	236	50	116	108	101	55	98
dip2 (°)	61	85	88	59	67	60	51	57
rake2 (°)	91	7	-3	103	106	83	64	90

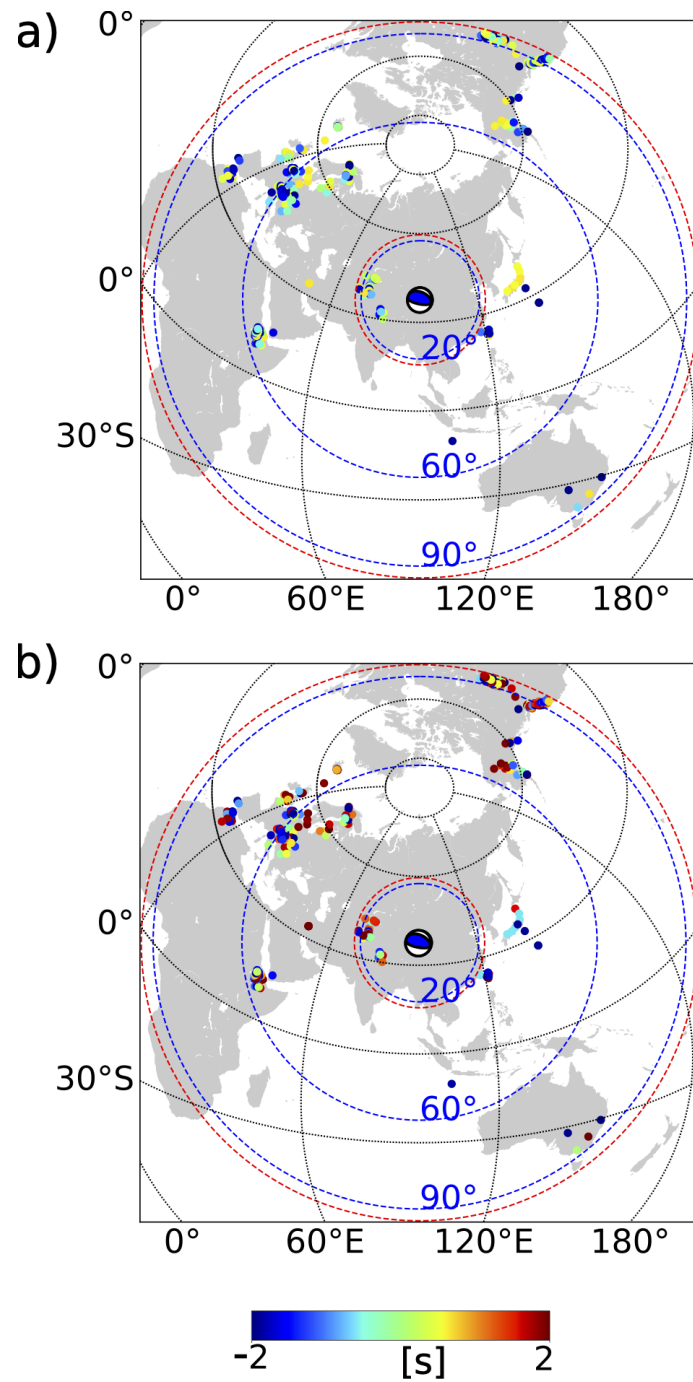


Figure S3: Empirical time shifts at virtual array stations for the P-phase for a) low-frequency and b) high-frequency backprojections that maximise the semblance of the reference event and are used for the backprojection. The color at each station indicates the time shift in seconds.

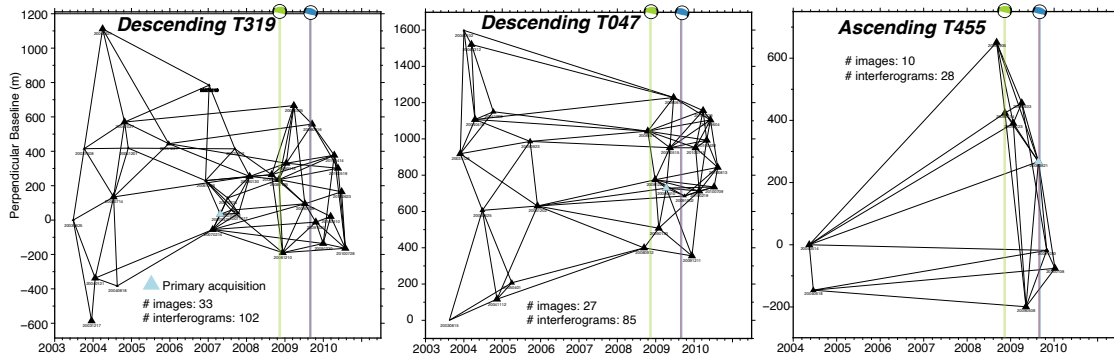


Figure S4: Computed interferograms for the three tracks. Triangles are SAR acquisitions with sizes according to their spatial extent. The "primary" images are shown with a blue triangle.

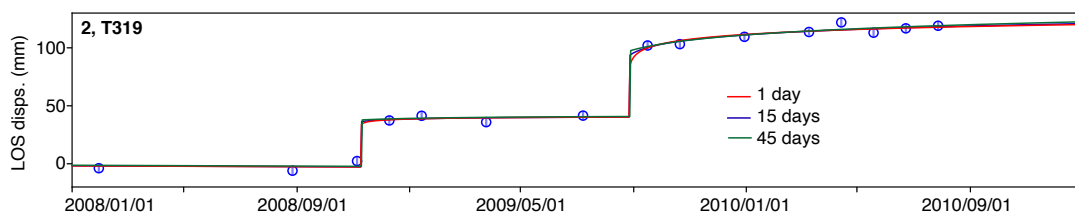


Figure S5: Time series of surface displacements from 2008 to 2011 for the pixel 2 of track 319 of Figure 2 (blue circles) with best-fitting estimations of long-term velocities, 2008, 2009 co-seismic offsets and logarithmic afterslip functions for three relaxations times (1 day in red, 15 days in blue and 45 days in green).

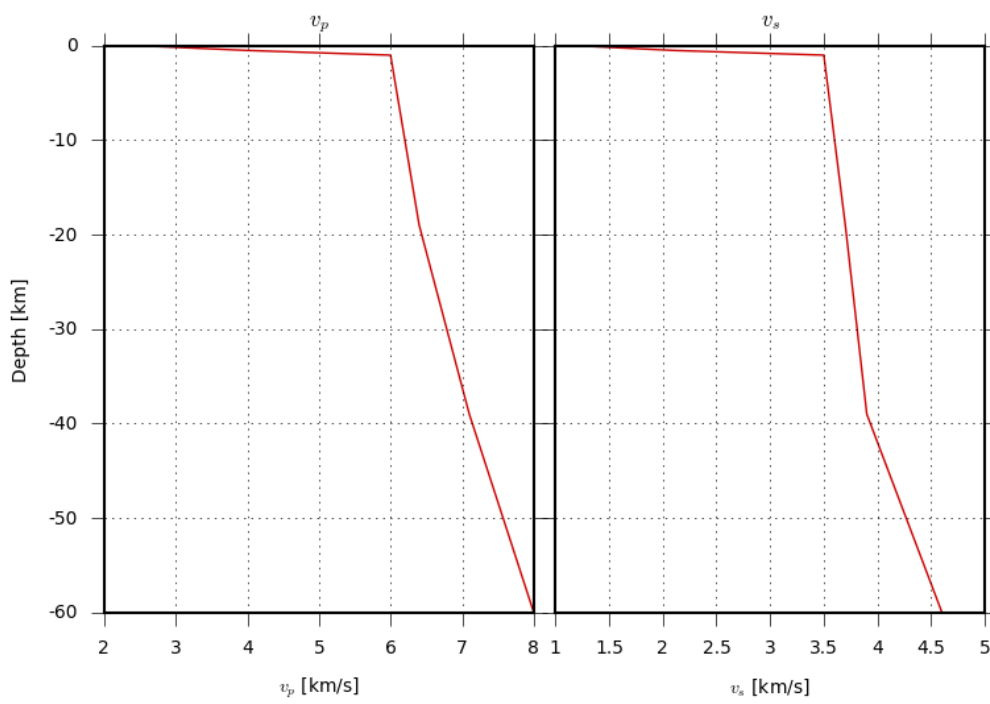


Figure S6: Crustal velocity model of the elastic stratified medium used to compute the near-field surface displacements.

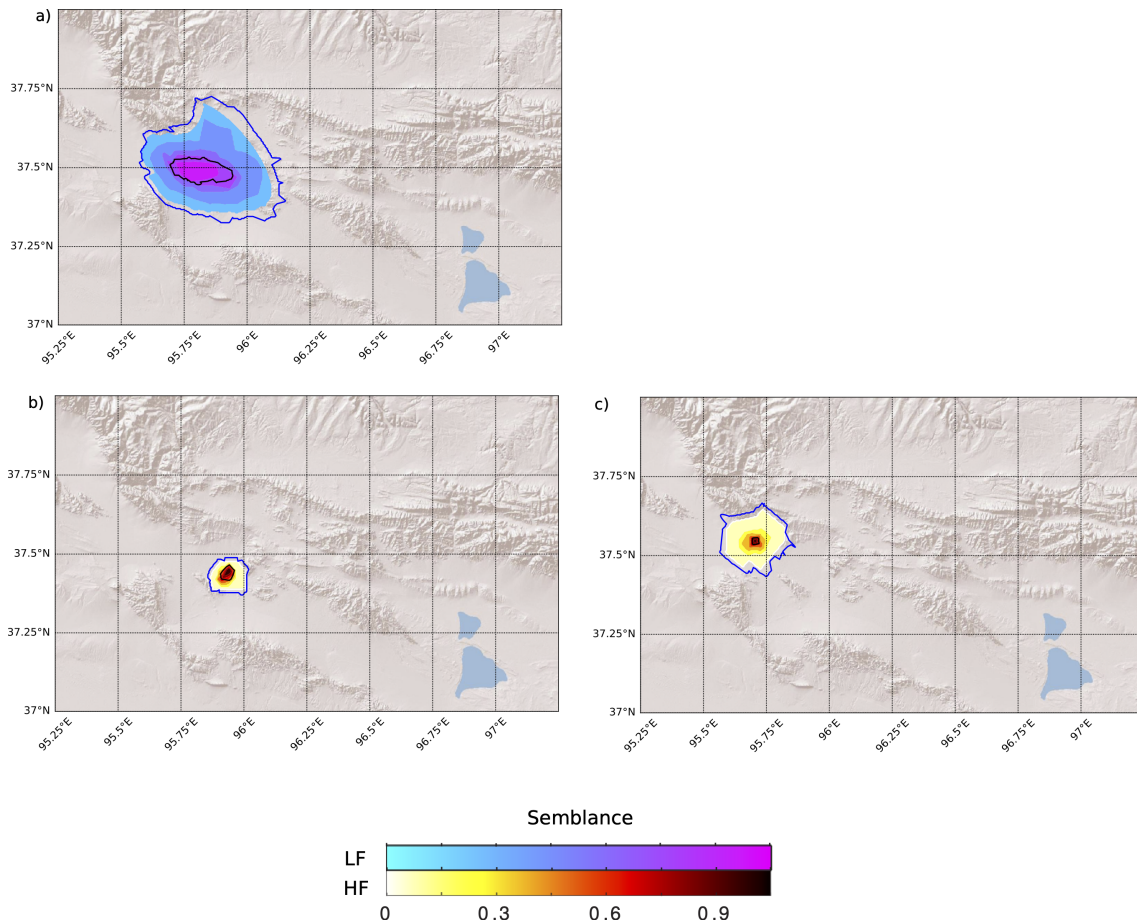


Figure S7: Semblance mapping for each time-steps for the 2008 Qaidam earthquake. Contour lines are colored after the cumulative semblance at any time-step. The black outlines represent the spatial uncertainty of 86% of the semblance values and the blue outlines the spatial uncertainty of 96% of the semblance values. They uncertainties are drawn as minimum bounding outlines for the locations of the semblance from 100 bootstrapped realisations of the semblance. a) Low-frequency semblance mappings for every time-step of 8 s and window length of 26 s individually. b-c) High-frequency semblance mappings for every time step of 2 s.

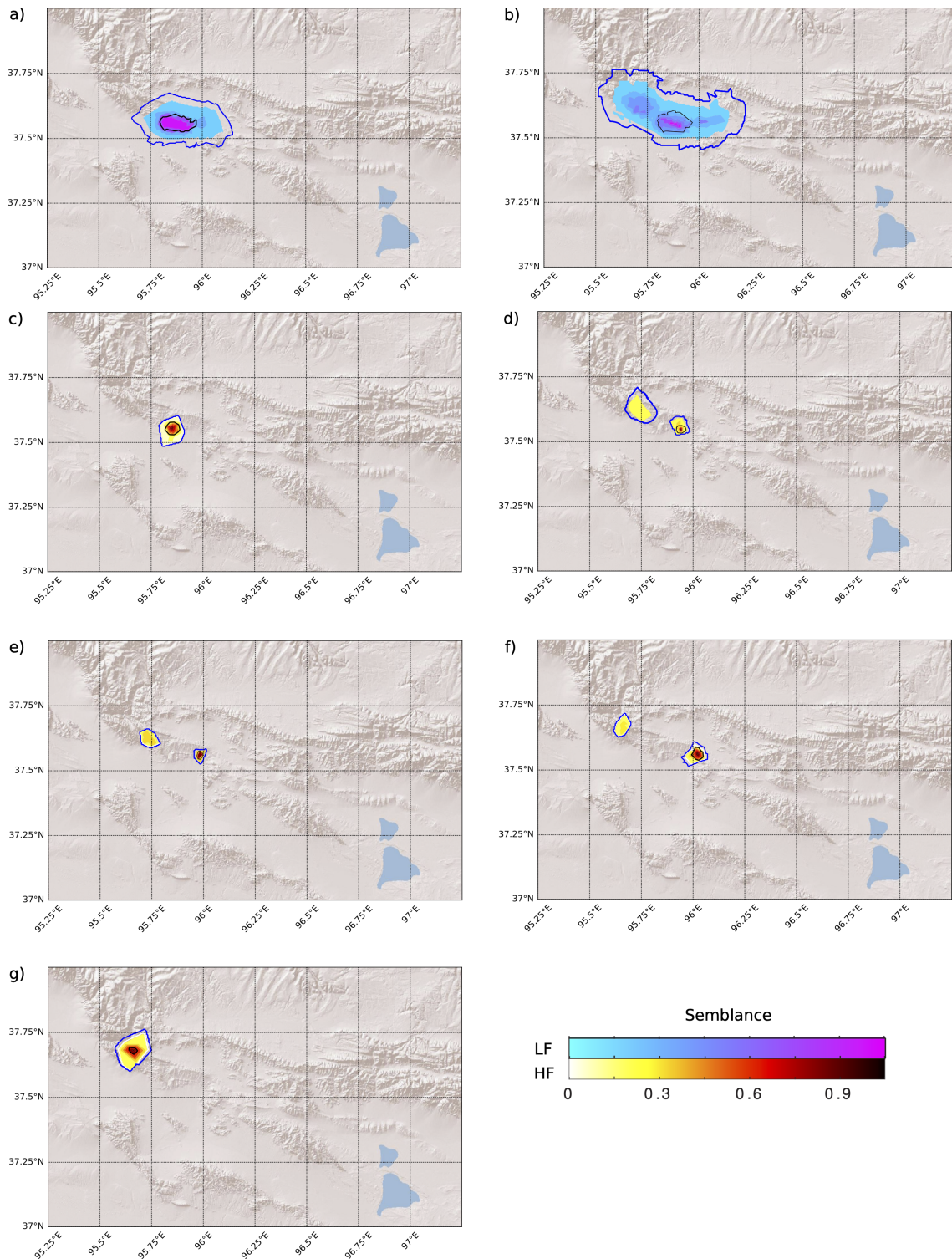


Figure S8: Semblance mapping for each time-step for the 2009 Qaidam earthquake, contour lines are colored after the cumulative semblance at any time-step. The black outlines represent the spatial uncertainty of 86% of the semblance values and the blue outlines the spatial uncertainty of 96% of the semblance values. They uncertainties are drawn as minimum bounding outlines for the locations of the semblance from 100 bootstrapped realisations of the semblance. The low-frequency semblance mappings for every time-step of 8 s and window length of 26 s individually in each of the subfigures a) and b). High-frequency semblance mappings for every time-step of 2 s individually in each of the subfigures c)-g).

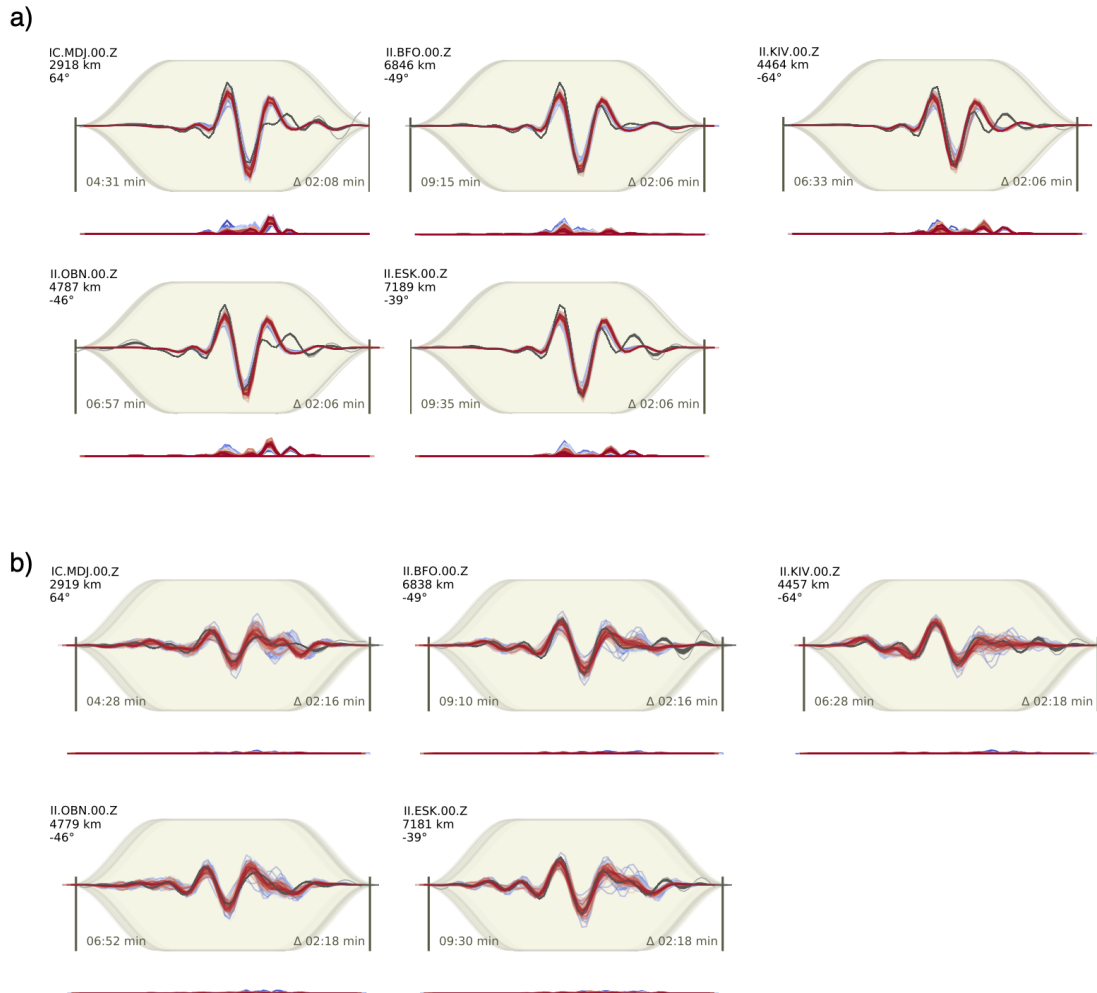


Figure S9: Waveform fits of the P-phase for the 2008 earthquake north-dipping solution (a) and the 2009 earthquake (b) for five random stations, which are common to both datasets. Restituted and filtered traces without tapering are in light grey while traces with tapering and processing are in dark grey. The filtered, tapered, and shifted synthetic traces for the 200 bootstraps are colored according to their misfit from red (best fit) to blue (worst fit). The amplitudes of the traces are scaled according to the weights (small weight, small amplitude) and normed relative to the maximum amplitude. The bottom panel shows residuals for all 200 bootstraps chains. Stations information (name with the component, distance to the source, azimuth of station with respect to the source) is given on the left-top. The background shaded area shows the applied taper function.

Table S2: Summary of the prior probabilities for the 2008 co-seismic rectangular fault inference \mathcal{U} defines normal distribution. Northing and Easting positions are relative to the gCMT solution.

Parameters	prior
Easting (km)	$\mathcal{U}(-2, 15)$
Northing (km)	$\mathcal{U}(0, 20)$
Depth (km)	$\mathcal{U}(2, 30)$
Length (km)	$\mathcal{U}(2, 30)$
Width (km)	$\mathcal{U}(.5, 30)$
Slip (m)	$\mathcal{U}(0.2, 3)$
Strike (°)	$\mathcal{U}(80, 310)$
Dip (°)	$\mathcal{U}(0, 80)$
Rake (°)	$\mathcal{U}(55, 135)$
Nucleation X	$\mathcal{U}(-1, 1)$
Nucleation Y	$\mathcal{U}(-1, 1)$
Velocity (m/s)	$\mathcal{U}(2000, 4000)$
Time (s)	$\mathcal{U}(-10, 10)$

Table S3: Summary of the prior probabilities for the 2008 post-seismic rectangular fault inference. Northing and Easting positions are relative to the gCMT solution.

Parameters	prior
Easting (km)	$\mathcal{U}(-2, 15)$
Northing (km)	$\mathcal{U}(0, 20)$
Depth (km)	$\mathcal{U}(2, 30)$
Length (km)	$\mathcal{U}(2, 30)$
Width (km)	$\mathcal{U}(.5, 30)$
Slip (m)	$\mathcal{U}(0.02, 1.5)$
Strike (°)	$\mathcal{U}(250, 310)$
Dip (°)	$\mathcal{U}(0, 80)$
Rake (°)	$\mathcal{U}(55, 135)$

Table S4: Summary of the prior probabilities for the 2009 co-seismic rectangular fault inference. The three sources are numerated 0 (middle), 1 (east) and 2 (west). Northing and Easting positions are relative to the gCMT solution.

Parameters	prior	Parameters	prior
Depth 0 (km)	$\mathcal{U}(.5, 10)$	Strike 0 (°)	$\mathcal{U}(80, 140)$
Depth 1 (km)	$\mathcal{U}(.5, 10)$	Strike 1 (°)	$\mathcal{U}(80, 140)$
Depth 2 (km)	$\mathcal{U}(.5, 10)$	Strike 2 (°)	$\mathcal{U}(100, 140)$
Dip 0 (°)	$\mathcal{U}(30, 70)$	Width 0 (km)	$\mathcal{U}(2, 9)$
Dip 1 (°)	$\mathcal{U}(30, 70)$	Width 1 (km)	$\mathcal{U}(2, 9)$
Dip 2 (°)	$\mathcal{U}(30, 70)$	Width 2 (km)	$\mathcal{U}(2, 9)$
Easting 0 (km)	$\mathcal{U}(-1, 2)$	Nucleation X0	$\mathcal{U}(-1, 1)$
Easting 1 (km)	$\mathcal{U}(6, 15)$	Nucleation X1	$\mathcal{U}(-1, 1)$
Easting 2 (km)	$\mathcal{U}(-15, -9)$	Nucleation X2	$\mathcal{U}(-1, 1)$
Length 0 (km)	$\mathcal{U}(6, 16)$	Nucleation Y0	$\mathcal{U}(-1, 1)$
Length 1 (km)	$\mathcal{U}(2, 10)$	Nucleation Y1	$\mathcal{U}(-1, 1)$
Length 2 (km)	$\mathcal{U}(2, 10)$	Nucleation Y2	$\mathcal{U}(-1, 1)$
Northing 0 (km)	$\mathcal{U}(-5, 9)$	Velocity 0 (m/s)	$\mathcal{U}(2000, 4500)$
Northing 1 (km)	$\mathcal{U}(-5, 9)$	Velocity 1 (m/s)	$\mathcal{U}(2000, 4500)$
Northing 2 (km)	$\mathcal{U}(2.5, 9)$	Velocity 2 (m/s)	$\mathcal{U}(2000, 4500)$
Rake 0 (°)	$\mathcal{U}(-180, 180)$	Time 0 (s)	$\mathcal{U}(-10, 10)$
Rake 1 (°)	$\mathcal{U}(-180, 180)$	Time 1 (s)	$\mathcal{U}(-10, 10)$
Rake 2 (°)	$\mathcal{U}(-180, 180)$	Time 2 (s)	$\mathcal{U}(-10, 10)$
Slip 0 (m)	$\mathcal{U}(0.2, 3)$		
Slip 1 (m)	$\mathcal{U}(0.2, 3)$		
Slip 2 (m)	$\mathcal{U}(0.2, 3)$		

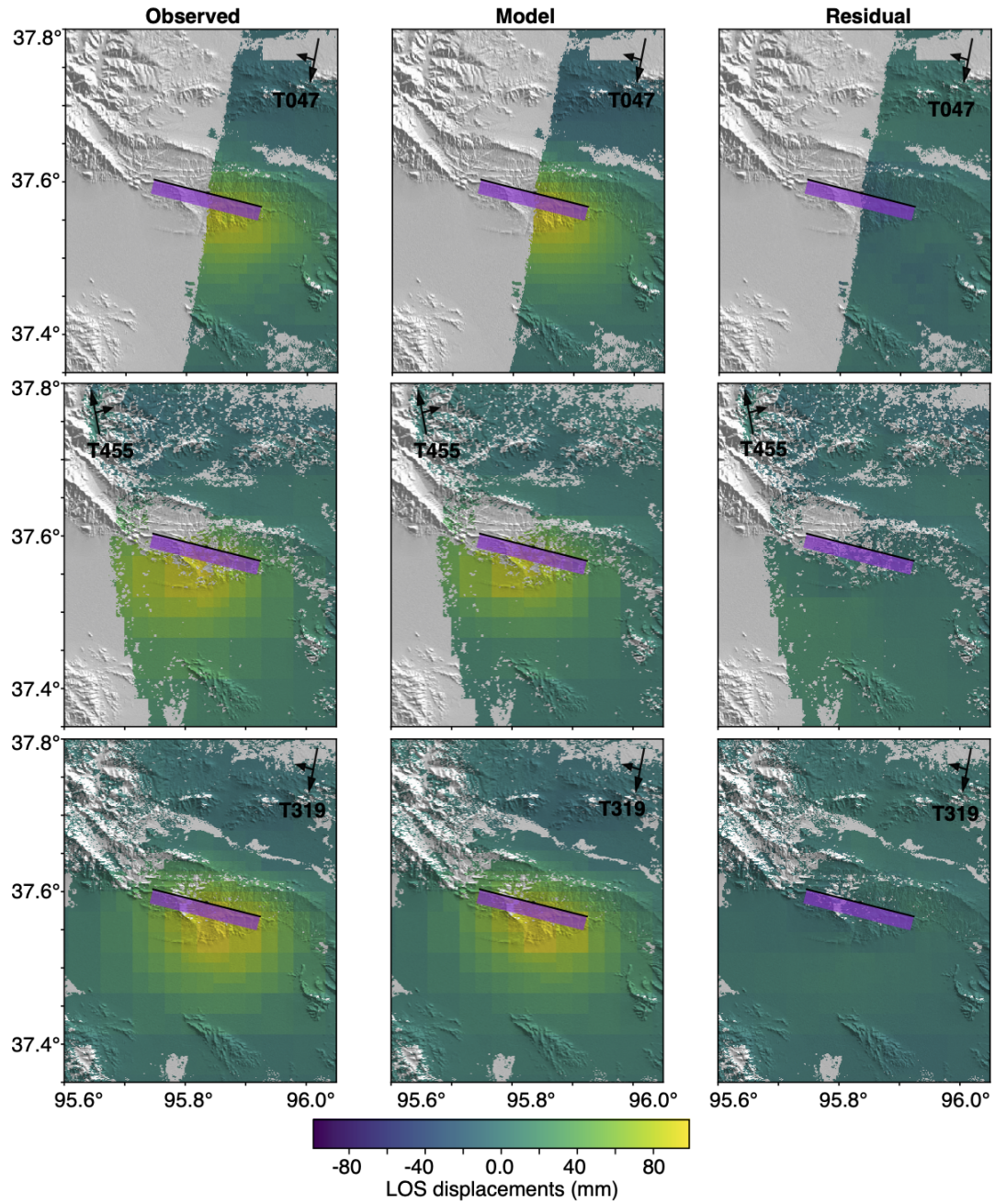


Figure S10: Comparison between data and model from the optimisation of one rectangular south-dipping fault in agreement with the 10th November 2008 earthquake data. Left: Sub-sampled surface displacements for tracks 319, 047 and 455. Middle: Modeled displacements associated with the maximum likelihood of the posterior probability distribution. Right: Residuals between the forward model and the observations.

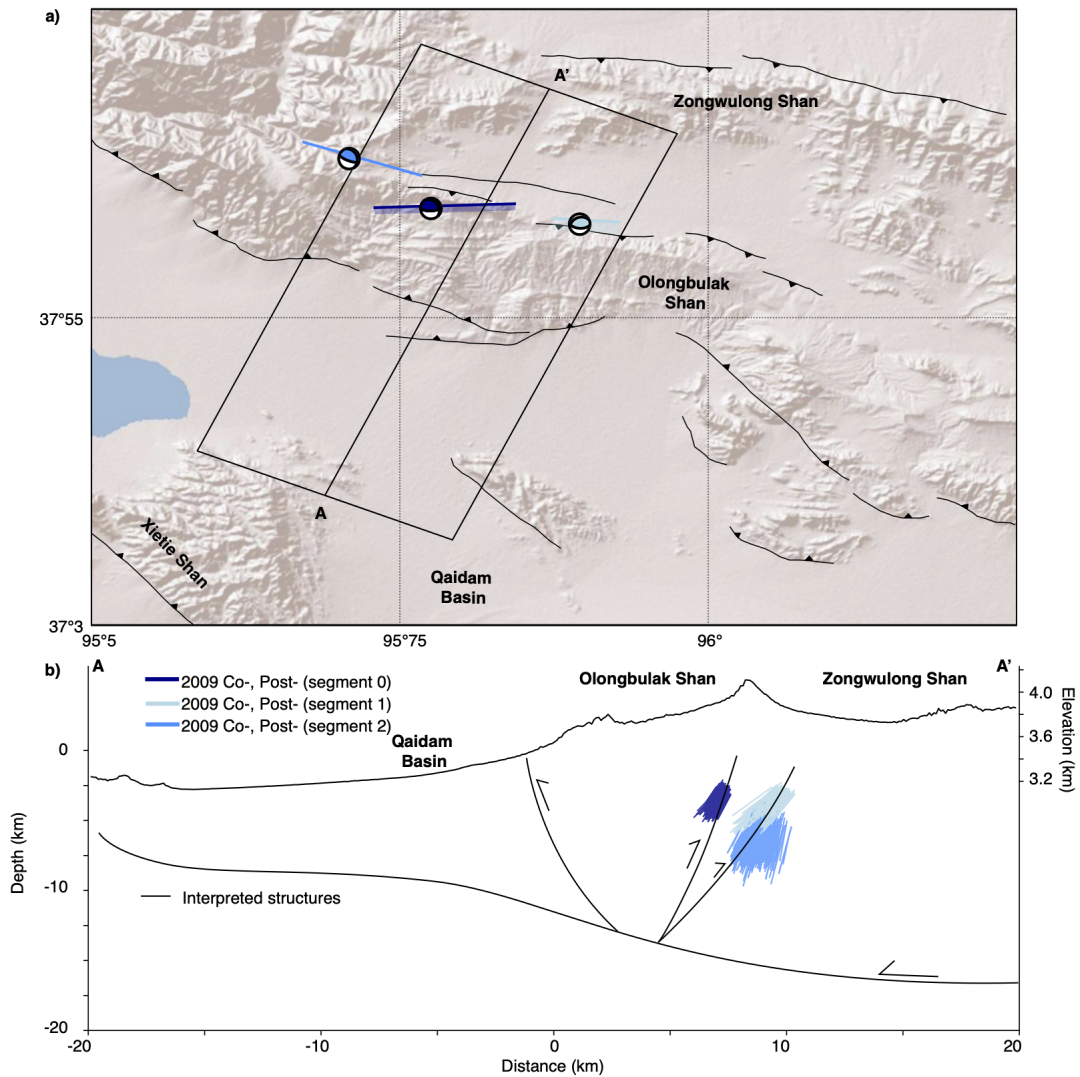


Figure S11: Posterior models for the 28th August 2009 earthquake obtained from the optimisation of three rectangular faults in agreement with a stack of co-seismic interferograms. a) Best-fitting posterior geometries in map view for the three segments of the 2009 co-seismic and post-seismic (dark blue, cyan, blue) source inferences. b) As for top figure, but along the N22°E profile perpendicular to the Olongbulak Shan marked AA' in (a) and with interpreted fault geometry at depth. Fault geometries are very similar to the three fault segments obtained from the optimisation of the co-seismic surface displacements from the time series data, suggesting that post-seismic slip occurred on similar fault planes than co-seismic slip.

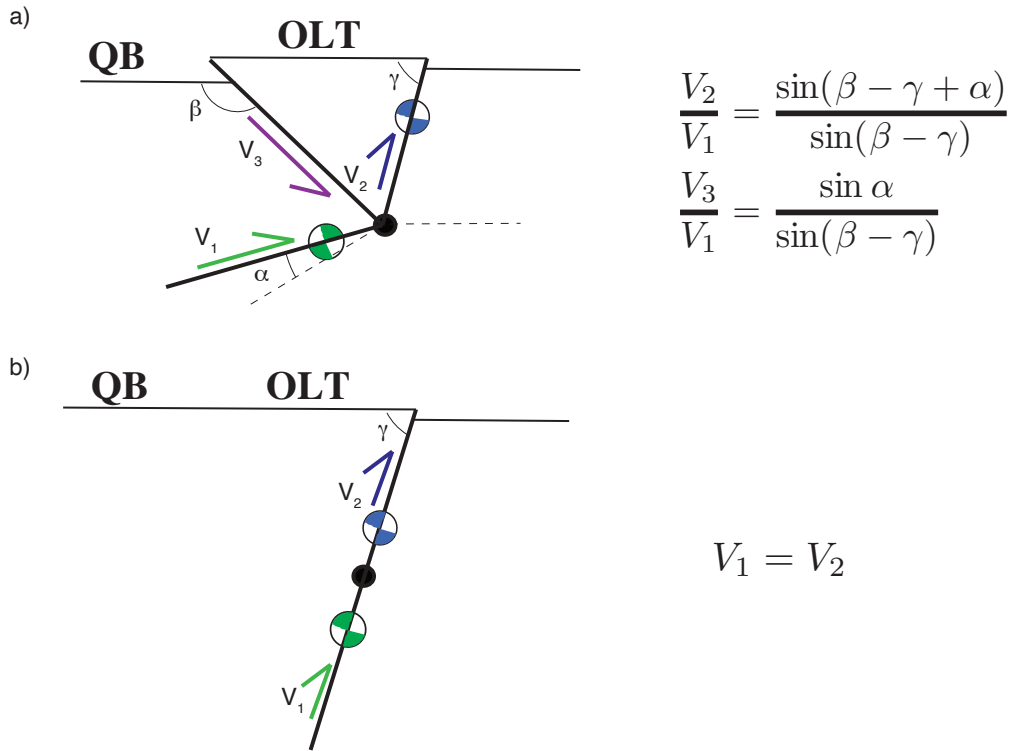


Figure S12: Conservation of the kinematic motion across the Olongbulak pop-up (OLT) for the south-dipping scenario. a) If the dip angle of the deep-seated fault, where the 2008 earthquake occurred ($\gamma - \alpha$), is smaller than the dip angle of the shallow high-angle fault, where the 2009 earthquake occurred (γ), then the change of dip angle between the two faults creates a differential of vertical uplift between the Qaidam Basin (QB) and the Olongbulak ranges accommodated by a shallow back-thrust fault dipping to the north ($180 - \beta$). Slip on each fault segment is controlled by the geometry with equations provided in [Daout et al. \[2016\]](#). b) If the deep-seated segment is coplanar to the shallow segment, then no back-thrust is kinematically required.

Table S5: Comparison of the variance-covariance estimations of the InSAR co-seismic Time Series (TS) data maps, co-seismic interferograms (IFG), and stack of co-seismic interferograms

		Variance (m ²)	Auto-covariance (m ²)	Correlation distance (m ²)
2008 Co- TS	T319	1.4×10^{-6}	1.7×10^{-6}	0.6
2008 Co- TS	T047	2.7×10^{-6}	3.8×10^{-6}	1.6
2008 Co- TS	T455	3.2×10^{-6}	3.7×10^{-6}	1.4
2008 Co- IFG	T319	3.2×10^{-6}	3.2×10^{-6}	1.1
2008 Co- IFG	T047	9.6×10^{-6}	9.0×10^{-6}	1.6
2008 Co- IFG	T455	4.2×10^{-6}	6.2×10^{-6}	0.7
2008 Stack	T319	3.7×10^{-6}	4.3×10^{-6}	1.1
2008 Stack	T047	1.1×10^{-5}	1.2×10^{-5}	1.2
2008 Stack	T455	9.8×10^{-6}	1.4×10^{-5}	1.8
2009 Co- TS	T319	1.0×10^{-6}	1.5×10^{-6}	1.2
2009 Co- TS	T047	2.3×10^{-7}	2.6×10^{-7}	1.3
2009 Co- TS	T455	1.6×10^{-6}	2.2×10^{-6}	2.2
2009 Co- IFG	T319	6.2×10^{-5}	6.8×10^{-5}	1.8
2009 Co- IFG	T047	6.4×10^{-6}	8.6×10^{-6}	0.9
2009 Co- IFG	T455	8.8×10^{-6}	8.9×10^{-6}	1.1
2009 Stack	T319	6.3×10^{-6}	7.2×10^{-6}	1.2
2009 Stack	T047	1.4×10^{-5}	1.4×10^{-5}	2.6
2009 Stack	T455	1.7×10^{-5}	1.8×10^{-5}	1.9

References

- Daout, S., S. Barbot, G. Peltzer, M.-P. Doin, Z. Liu, and R. Jolivet, Constraining the kinematics of metropolitan Los Angeles faults with a slip-partitioning model, *Geophys. Res. Lett.*, 2016.
- Ekström, G., M. Nettles, and A. Dziewoński, The global CMT project 2004–2010: Centroid-moment tensors for 13,017 earthquakes, *Physics of the Earth and Planetary Interiors*, 200, 1–9, 2012.